Contributed Paper

High Power Electron Heating Experiments at the Plug Region of GAMMA 10

SAITO Teruo, ISHII Kameo, ITAKURA Akiyoshi, ICHIMURA Makoto, ISLAM Md. Khairul, KATANUMA Isao, KOHAGURA Junko, TATEMATSU Yoshinori, NAKASHIMA Yousuke, NUMAKURA Tomoharu, HIGAKI Hiroyuki, HIRATA Mafumi, HOJO Hitoshi, YOSHIKAWA Masayuki, SAKAMOTO Keishi[1)], IMAI Tsuyoshi, CHO Teruji and MIYOSHI Syoichi

Plasma Research Center, University of Tsukuba, Tsukuba, Ibaraki 305-8577, Japan

[1)]Naka Fusion Research Establishment, JAERI, Naka, Ibaraki 311-0193, Japan

(Received 25 November 2004 / Accepted 17 February 2005)

In the GAMMA 10 tandem mirror, a high power ECRH experiment at the plug region is now in progress. As the first step of this experiment, high power operation of existing gyrotrons for plug ECRH has been carried out at a power P_{plug} exceeding their nominal powers of 200 kW. In this step, the highest recorded value of the axial ion confining potential φ_c for a hot ion mode plasma is 1.4 kV at P_{plug} = 240 kW. Then, in the second step, a newly developed high power gyrotron has been installed at one side of the both end plugs. The value of φ_c increased with P_{plug} and attained 2.1 kV at P_{plug} = 370 kW. The potential difference $\Delta\Phi$ from the plug potential to the end plate potential exceeded 5 kV. The effective temperature T_{eff} as a mean energy of the end loss electrons reached 3 keV, and the scaling between $\Delta\Phi$ and T_{eff} has been expanded. Functions of the plug ECRH on electrons are studied from the viewpoint of velocity space diffusion, and a picture of ECRH-induced axial electron motion is presented.

Keywords:

ECRH, tandem mirror, GAMMA 10, potential distribution, velocity space diffusion

1. Introduction

In the GAMMA 10 tandem mirror, fundamental ECRH at the plug region (plug ECRH) generates the axial ion confining potential φ_c [1]. Experimental observation shows that φ_c increases with the plug ECRH power, and no saturation has thus far been observed as long as the electron density is kept at a certain level. Thus, it is expected that φ_c will further increase with higher power ECRH at the plug region. To meet this expectation, a high power electron heating experiment is now in progress. The objectives of this experiment are formation of φ_c as large as possible, study of the physical mechanism of potential generation in a wide potential range, and formation of a large radial potential gradient to improve radial confinement by suppressing fluctuations [2]. Among these objectives, this paper reports high potential generation with high power electron heating. At the same time, the present paper studies an axial electron flow as an important factor of the axial potential structure from the viewpoint of ECRH in a mirror field.

As the first step of this plan, high power operation of existing gyrotrons for the plug ECRH has been carried out at a power exceeding their nominal power of 200 kW. A new record value of φ_c was obtained in this step. Then, as the second step, a newly developed high power gyrotron was installed at one side of both end plugs, and a much higher value of φ_c = 2.1 kV was achieved with this gyrotron [3]. This confirms that the ion confining potential increases with the ECRH power. While this value is sufficient for a parallel ion temperature of several hundred eV in the present experiment, the necessary value of φ_c depends on the ion temperature. The required ECRH power for higher φ_c is discussed in Ref. [4].

For efficient generation of high potentials with high power heating, a clear understanding of the process of electron heating is very important. The plug ECRH drives a portion of the heated electrons into the loss cone and induces an intense axial flow of warm electrons. This axial electron flow is a key factor in the whole axial potential distribution [5-7]. Thus, the study of this electron flow is of great importance in the high power heating regime. A portion of the axially flowing electrons is observed as end loss electrons. From measurement of the end loss electrons, a valuable measure of electron heating is provided and the effects of high power heating on potential generation are evaluated. In fact,

author's e-mail: saito@prc.tsukuba.ac.jp

This article is based on the invited talk at the JSPF 21st Annual Meeting (2004, Shizuoka).

the effective temperature T_{eff} as a mean energy of the end loss electrons is a good scaling factor of the axial potential distribution, and an empirical scaling between $\Delta\Phi = \Phi_P - \Phi_{EP}$ and T_{eff} has been obtained [8]. Here, Φ_P is the plug potential and Φ_{EP} is the end plate potential. The high power heating experiment has expanded this scaling [9].

The plug ECRH has two functions on electrons by driving two types of velocity space diffusion. The first type of diffusion enhances mirror reflection beyond the plug position, which results in the plug potential. The second type of diffusion creates the axial electron flow. This paper discusses formation of the electron flow from the viewpoint of the resonance condition and propagation of the heating wave. In particular, observations on the origin of the low and high temperature components of the end loss electrons are presented.

The outline of the present paper is as follows. The next section briefly describes the experimental setup. Section **3** presents generation of high potentials. High power electron heating examined from the measurement of end loss electrons is reported in this section. ECRH-induced velocity space diffusion of electrons is discussed in Sec. **4**. Section **5** summarizes this paper.

2. Experimental Setup

This section gives a brief description of the region from the plug to the end plate of GAMMA 10. More details of the experimental setup are provided in Refs. [5, 10]. Figure 1 shows the axial distributions of the on-axis magnetic field strength and a typical electrostatic potential. Fundamental ECRH (plug ECRH) is applied at the plug position between the mid plane (B = 0.5 T) and the outer mirror throat (B_m = 3.0 T, potential Φ_m) of the end mirror cell. The magnetic field strength at the plug position is B_p = 1 T. In addition to the plug ECRH, second harmonic ECRH is applied to the mid-plane of the end mirror cell. For simplicity, Fig. 1 indicates only the plug ECRH.

The new high power gyrotron is installed for the west side plug ECRH. Microwave power with a frequency of 28 GHz delivered in a Gaussian-like pattern through a vacuum window is coupled to the HE_{11} mode in a corrugated waveguide with diameter of 63.5 mm and transmitted into the vacuum vessel of GAMMA 10. Then, the microwave power of linear polarization is radiated by using profile-tailoring mirrors. The radiated power is mostly coupled to the X-mode for the present geometry. The radiation pattern on the resonance layer is nearly axi-symmetrized. The design of the mirrors will be published elsewhere. The east side plug ECRH is carried out with high power operation of an existing gyrotron at the moment. The microwave power delivered from this gyrotron is transmitted in TE_{02} mode through circular waveguides and radiated to the plasma with a combination of a Vlasov-Nakajima antenna and a cylindrical mirror. The radiation pattern is also axi-symmetrized [10]. An array of open-ended rectangular waveguide (WR-28) (waveguide array) is installed to measure the microwave power transmitted through the resonance layer.

The potential Φ_C near the mid-plane of the central cell and the potential Φ_B at the mid-plane of the end mirror cell are measured with gold neutral beam probes [11]. The plug potential Φ_P is evaluated from the energy spectrum of the end loss ions [12]. An end plate of stainless steel is installed on the end wall of the vacuum vessel. The magnetic field strength at the end plate is 0.01 T. The end plate is connected to the vacuum vessel through a large resistance, and it is electrically floating with potential Φ_{EP}. End loss electrons are measured with a multi-grid type electrostatic energy analyzer located behind a small mesh-covered hole of the end plate [13].

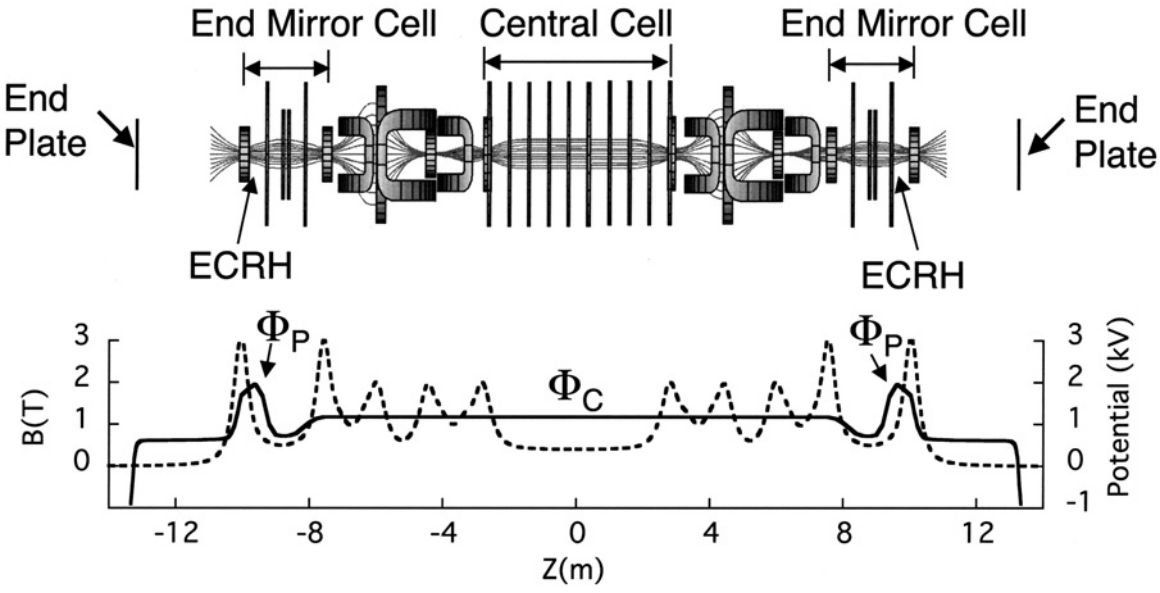

Fig. 1 Axial distributions of the on-axis magnetic field strength (dashed line) and a typical electrostatic potential (solid line). The plug ECRH is applied at the plug position (B = 1.0 T, potential Φ_P) between the mid plane (B = 0.5 T, potential Φ_B) of the end mirror cell and the outer mirror throat (B_m = 3.0 T, potential Φ_m). Only the plug ECRH is shown for simplicity.

3. Experimental Results of High Power Electron Heating

3.1 High potential generation

The GAMMA 10 experiment has two modes of plasma production: the hot ion mode [14,15] and the high potential mode [16,17]. In the hot ion mode, plasma is produced and sustained with an ICRF wave of the fast wave branch radiated from the NAGOYA type III antennas located at both ends of the central cell. Another ICRF wave of the slow wave branch excited by a double half turn antenna heats the central cell ions. The electron density n_{ec} in the central cell is in the range of $(2 - 3) \times 10^{12}$ cm^{-3}, and the ion temperature perpendicular to the magnetic field T_{ic} is several keV. In the high potential mode, fundamental (plug) and second harmonic (barrier) ECRH applied in the end mirror cell produce plasma. The slow wave is also applied for ion heating. A typical value of n_{ec} is in the order of 10^{11} cm^{-3}, and T_{ic} is hundreds of eV. The electron density at the plug region is in the order of 10^{10} cm^{-3} to 10^{11} cm^{-3} during plugging.

Figure 2 (a) shows the time variations of Φ_P, Φ_C, and Φ_B obtained from a hot ion mode plasma in the second step experiments. The plug ECRH is turned on after the plasma reaches a steady state. On application of the plug ECRH, the plasma potentials measured from the vacuum vessel show step-like changes. This indicates a quick response of electrons to ECRH. The plug potential is determined at intervals because it is evaluated from the energy spectrum of the end loss ions, which is measured by sweeping the repeller voltage of the energy analyzer. The value of Φ_P becomes the largest of the potentials along the magnetic field line, and a large ion confining potential $\varphi_c = \Phi_P - \Phi_C$ is generated by the plug ECRH. Figure 2 (b) denotes the line density in the central cell and the end loss ion flux. The end loss ion flux strongly decreases, and, consequently, the line density in the central cell shows a clear increase during the plug ECRH. Because the pulse width of the new gyrotron is rather limited at the moment, the line density does not reach a saturation level during the ECRH pulse.

The increment in Φ_P strongly depends on the plug ECRH power P_{plug}. Figure 3 plots the central cell potential Φ_C and the barrier potential Φ_B in addition to Φ_P for four different cases, (a) without plug ECRH injection (downward triangles),

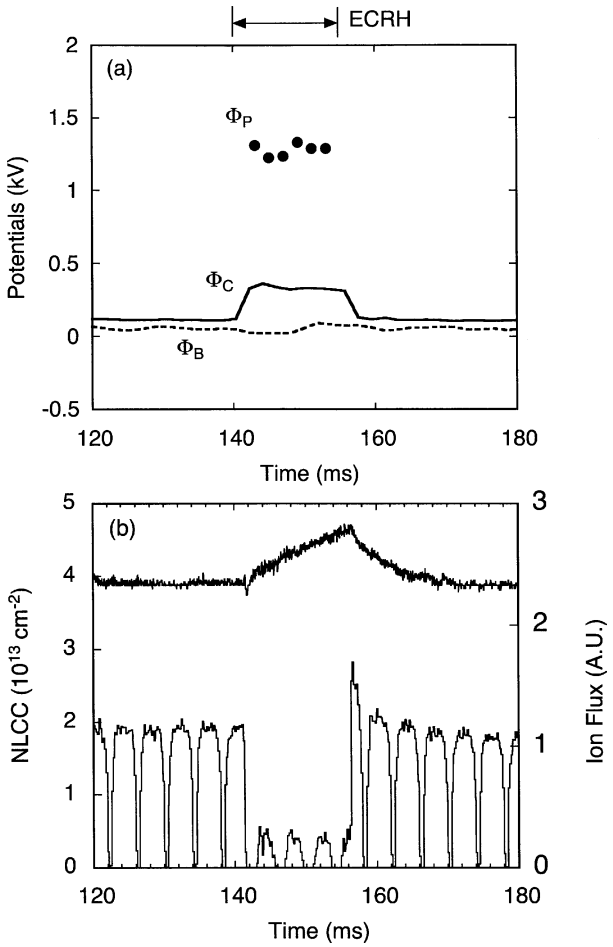

Fig. 2 (a) Time variations of Φ_P, Φ_C and Φ_B obtained from a hot ion mode plasma in the second step experiments. The heating power of the west plug ECRH is 300 kW in this shot. (b) The line density in the central cell and the end loss ion flux.

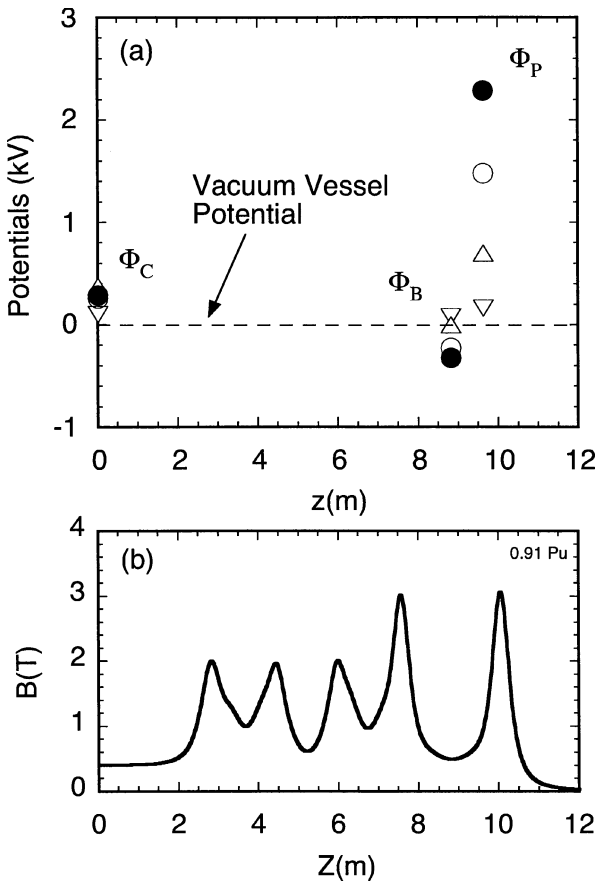

Fig. 3 The central cell potential Φ_C, the barrier potential Φ_B and the plug potential Φ_P are plotted for four different cases, (a) without plug ECRH injection (downward triangles), (b) low power experiment with of 130 kW (upward triangles), (c) the first step experiment with P_{plug} of 240 kW (open circles) and (d) the second step experiment with P_{plug} at the west side plug of 370 kW (closed circles). Each value is measured in reference to the vacuum vessel.

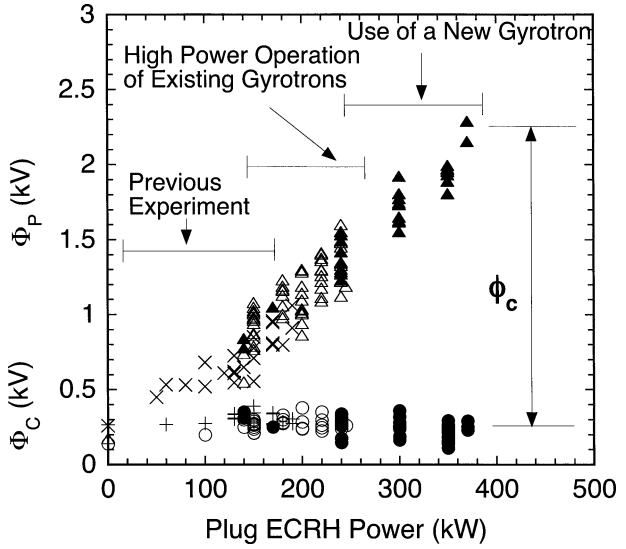

Fig. 4 Φ_P and Φ_C are plotted as functions of P_{plug}. Data are taken from the three stages of the GAMMA 10 experiment: data from the previous experiment (denoted with crosses), data from the first step experiment (open triangles), and data from the second step experiment with the new high power gyrotron (closed triangles).

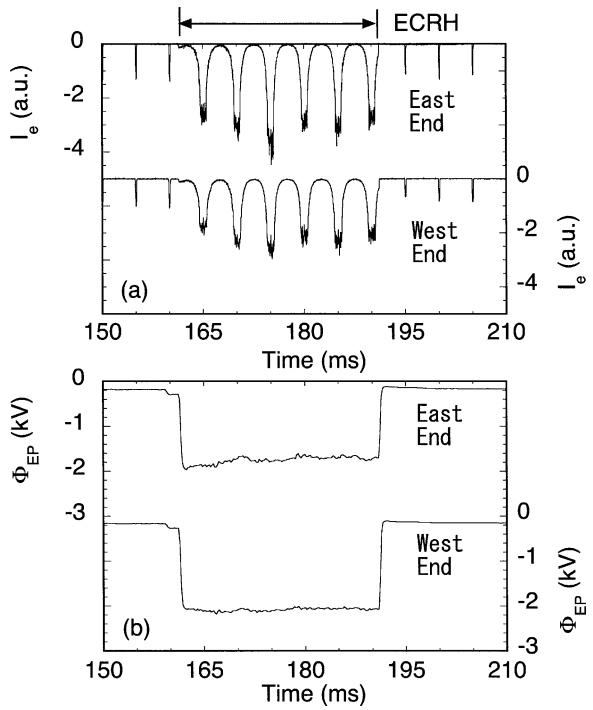

Fig. 5 (a) The end loss electron fluxes measured with the electrostatic energy analyzers located at both ends are shown. The pulse train is due to sweeping of the electron repeller voltage for energy analysis. The envelope indicates the electron flux. (b) The end plate potentials at both ends for the same shot as in Fig. (a) are plotted.

(b) low power experiment with P_{plug} of 130 kW (upward triangles), (c) the first step experiment with P_{plug} of 240 kW (open circles), and (d) the second step experiment with P_{plug} at the west side plug of 370 kW (closed circles). Data points plotted in Fig. 3 are obtained from hot ion mode plasmas. The plug potential increases with P_{plug}, while the variation of the central cell potential Φ_C is not so large. Thus, φ_c increases with Φ_P, which increases with P_{plug}. Figure 4 plots Φ_P and Φ_C obtained from the three stages of the high power heating experiment: data before high power heating (denoted with crosses), data from the first step experiment (open triangles), and data from the second step experiment (closed triangles). The attainable value of Φ_P increases with P_{plug}. Although the second step experiment has just started, the highest value of Φ_P has been attained. Thus, we can expect to generate still larger potentials with higher power operation of the new gyrotron. The maximum values of φ_c at the respective stages are 0.8 kV, 1.4 kV, 2.1 kV, respectively. The value of 2.1 kV is the highest recorded one in the hot ion mode.

3.2 End loss electrons and expansion of scaling

The plug ECRH generates $\varphi_c = \Phi_P - \Phi_C$. Another characteristic potential difference along the magnetic field line is formed between Φ_P and Φ_{EP}. Generation of this potential difference is closely connected with an ECRH-induced axial flow of warm electrons. A portion of the electrons of this flow have energies to overcome negative Φ_{EP} and appear as end loss electrons. Thus, measurement of end loss electrons provides valuable information about the axial electron flow.

Figure 5 (a) denotes the end loss electron flux measured with the electrostatic energy analyzers located at both ends. The pulse train is due to sweeping of the electron repeller voltage for energy analysis. The envelope indicates the electron flux. The ECRH-induced end loss electrons are observed at both ends with almost the same parameters. Figure 5 (b) shows the end plate potential Φ_{EP} at both ends for the same shot as that shown in Fig. 5 (a). The end plate potential becomes deeply negative to the vacuum vessel potential during the plug ECRH. The potential difference $\Delta\Phi = \Phi_P - \Phi_{EP}$ works as the confining potential for the ECRH-induced axially flowing electrons. It attains several kV during high power plug ECRH.

Figure 6 shows examples of current-voltage characteristics of the end loss electrons for low (140 kW) and high (300 kW) P_{plug} at the west plug. The heating power at the east plug is kept at 140 kW. The abscissa stands for the absolute value of the electron repeller voltage V_{rep} (< 0). The electron flux is constant while $|V_{rep}|$ is smaller than $|\Phi_{EP}|$ because the end plate in front of the analyzer works as an effective electron repeller grid. While the V-I characteristics have a multi-component feature, they are well fitted to a two-component Maxwellian with a lower temperature T_L and a higher temperature T_H [13]. The effective temperature, defined as $T_{eff} = (1 - \beta)T_L + \beta T_H$, represents the mean energy of the end-loss electrons. Here, β is the flux fraction of the T_H component evaluated at $V_{rep} = \Phi_{EP}$. As shown in Fig. 6, the flux of higher energy electrons significantly increases for high power heating.

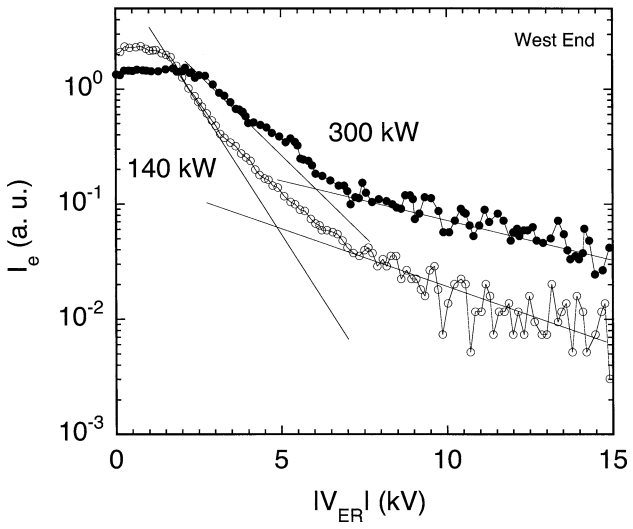

Fig. 6 The current-voltage characteristics of the end loss electrons for low (140 kW) and high (300 kW) P_{plug} at the west plug are indicated. The heating power at the east plug is kept at 140 kW. The abscissa stands for the absolute value of the electron repeller voltage V_{rep} (< 0).

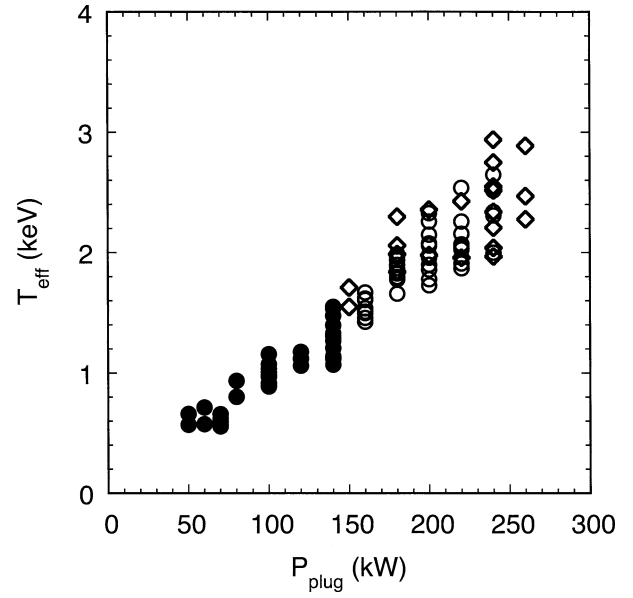

Fig. 7 The effective temperature of the end loss electrons T_{eff} is plotted as a function of P_{plug}. The closed circles indicate data obtained with P_{plug} below the nominal power. The open symbols denote data obtained from high P_{plug} experiments. Open circles stand for T_{eff} from the hot ion mode plasma and open diamonds represent those from the high potential mode plasma.

Figure 7 plots T_{eff} as a function of P_{plug}. The characteristics of the end loss electrons depend on heating at both sides. Thus, we present data of T_{eff} from the first step experiment because, in the second step experiment, the new gyrotron is installed at the west side only and, at the moment, the heating power at the east side is lower. The closed circles indicate data obtained in previous experiments with normal

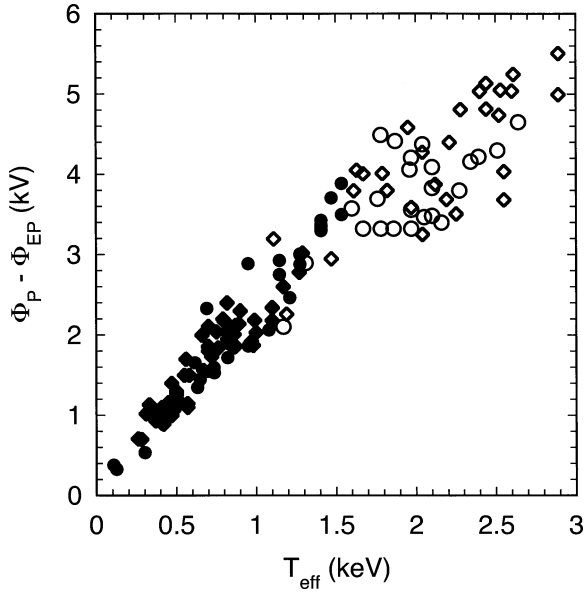

Fig. 8 Scaling law between $\Phi_P - \Phi_{EP}$ and T_{eff}. The closed circles indicate data obtained with P_{plug} below the nominal power. The open symbols stand for the high power heating. In addition, open circles denote $\Delta\Phi$ from hot ion mode plasmas and open diamonds represent those from high potential mode plasmas.

operation of gyrotrons. The open symbols denote data obtained from high P_{plug} experiments. Open circles stand for T_{eff} from the hot ion mode plasma and open diamonds represent those from the high potential mode plasma. Excepting some scattering due to shot-to-shot variation of the plasma condition, T_{eff} almost linearly increases with P_{plug} as long as the electron density is kept nearly constant.

An empirical scaling law between $\Delta\Phi = \Phi_P - \Phi_{EP}$ and T_{eff} has been presented [8]. The high power heating experiment has expanded this scaling. Figure 8 plots $\Delta\Phi$ as a function of T_{eff}. The closed circles indicate data obtained with existing gyrotrons of P_{plug} below 200 kW. The open symbols stand for data attained in the high power heating experiment. The value of $\Delta\Phi$ increases almost linearly with T_{eff}. Thus, predominance of the ECRH-induced axial electron flow over the axial potential distribution is also the case in the high power heating regime. In addition, open circles denoting $\Delta\Phi$ from the hot ion mode plasma and open diamonds representing those from the high potential mode plasma obey the same relation. Although potentials measured from the vacuum vessel are different in the two experimental modes, the relation between $\Delta\Phi$ and T_{eff} is the same in the two modes.

4. Functions of the Plug ECRH

4.1 ECRH-induced diffusion of electrons in velocity space

For efficient generation of high potentials with high power heating, understanding the process of electron heating is necessary. In particular, identification of the origins of the T_L and T_H components is very important. In this section, we

present a picture of the heating process.

Figure 9 denotes the velocity space of electrons with energy ε and magnetic moment μ. The variation of magnetic moment $\Delta\mu$ of electrons heated at the resonance position of $B = B_P$ leads to the change in energy by $B_P\,\Delta\mu$. Thus, heated electrons move along heating characteristics $\varepsilon = \mu B_P + \varepsilon_0$ in velocity space ($B_P < B_m$) [18,19]. Electrons in the region below the line $\mu B_{EP} - e\Phi_{EP}$ are confined by negative Φ_{EP}, and electrons right to the line $\mu B_m - e\Phi_m$ are magnetically trapped in the end mirror cell. Plasma is produced in the central cell region and flows out to the machine ends along magnetic field lines. Cold electrons in this flow locate in the lower part of region I, shown in Fig. 9. The net flow of electrons is in the direction from region I to region II (diffusion (1)). Electrons driven into region II are trapped in the end mirror cell, then mirror reflection of electrons is enhanced owing to the diffusion (1) and leads to generation of the plug potential that reflects the flowing ions to maintain charge neutrality [20,21]. This is the one of the two functions of the plug ECRH.

The heated electrons form a group of warm electrons. Electrons just below the line $\mu B_{EP} - e\Phi_{EP}$ are reflected by negative Φ_{EP} and travel back and forth between the end plates on the two sides. The axial electron flow consists of these electrons. A portion of the electrons below this line enter the loss region owing to acceleration by ECRH (diffusion (2)). Thus, the end plates at both ends are electrically connected by the axial electron motion. In fact, experimental values of Φ_{EP} at both ends are usually almost the same during the plug ECRH. Electrons below the line $\mu B_m - e\Phi_m$ in region III are magnetically trapped in the end mirror cell. A portion of these electrons move into the loss region owing to deceleration by ECRH (diffusion (3)). Diffusions (2) and (3) produce the end loss electrons. This is the other function of the plug ECRH. Then, the potential difference $\Phi_P - \Phi_{EP}$ is generated as the electron confining potential that scales with the mean energy T_{eff}.

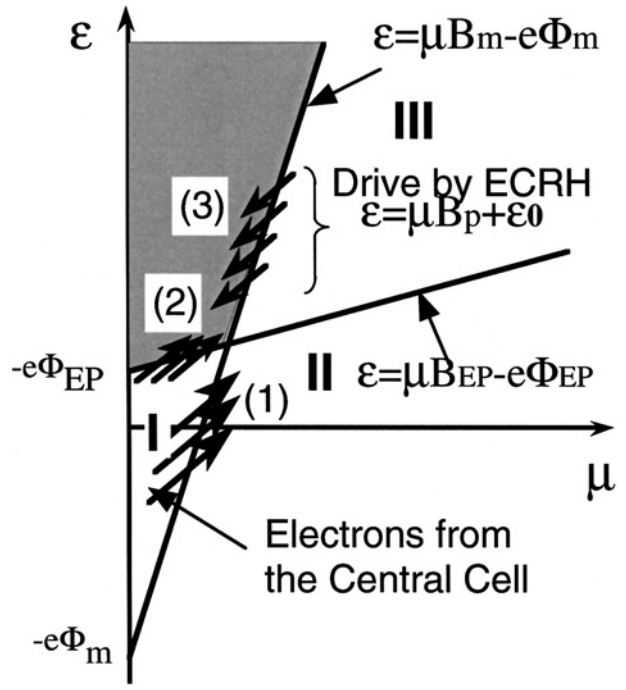

Fig. 9 A picture of ECRH-induced velocity space diffusion of electrons is denoted.

4.2 Resonance condition

Direction of electron drive to either of the two sides is determined from the resonance condition. The non-relativistic resonance condition is given by

$$k_{\parallel} v_{\parallel} = \omega - \omega_{ce} \tag{1}$$

where symbols with their usual meanings are used. The sign of $k_{\parallel} v_{\parallel}$ depends on the position of resonant interaction. Because the heating wave is injected from the high field side, the parallel wave number $k_{\parallel}$ is directed to the mid-plane of the end mirror cell. Thus, for high field side interaction, $\omega_{ce} > \omega$, the direction of the parallel electron velocity $v_{\parallel}$ should be opposite to $k_{\parallel}$ and only electrons moving to the outer mirror throat resonate with the heating wave. For low field

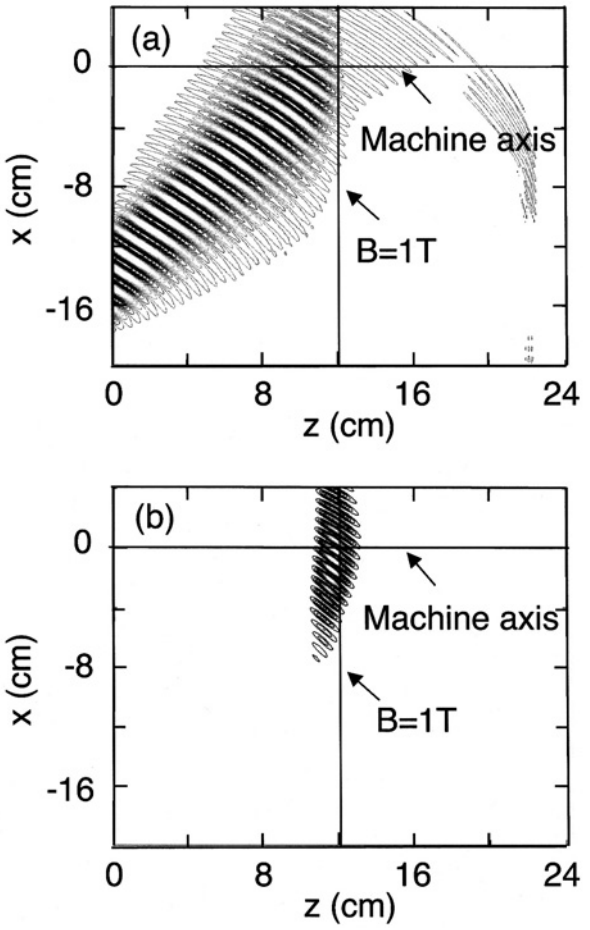

Fig. 10 Propagation of the heating wave calculated by using a full Maxwellian code is shown. The heating wave is launched from the high field side and propagates up right with the same angle to the machine axis as that in experiment. It is excited in linear polarization along the y direction. (a) The amplitude distribution of the E_y component of the wave electric field. (b) Wave absorption profile. The two profiles plotted in Figs. (a) and (b) stand for snap shots at a certain instant.

side interaction, $\omega_{ce} < \omega$, on the other hand, the direction of $v_{\parallel}$ should be the same as $k_{\parallel}$ and only electrons traveling towards the central cell resonate with the heating wave. Diffusion (1) of high field side interaction results in magnetic reflection of electrons emanating from the central cell and generation of plug potential. Diffusions of (2) and (3) of high field side interaction lead to direct electron loss to the end plate of the same side as the plug region under heating. Diffusions of (2) and (3) stemming from low field side interaction drive electrons to the end opposite the heating side.

High field side interaction always occurs. However, occurrence of low field side interaction depends on the electron density. Recently, a numerical code of electromagnetic wave propagation applicable to beach geometry has been developed [22]. This code includes cyclotron absorption. Calculation with this code shows that for a typical density regime of the plug region of GAMMA 10, microwave power launched from the high field side is not fully absorbed before the resonance layer and a finite fraction penetrates into the low field side [23]. Figure 10 depicts wave propagation calculated by using this code. The magnetic field profile and the density distribution simulate the plug region. A heating wave with frequency of 28 GHz is launched from the high field side in linear polarization with an angle to the machine axis the same as that in the experiment. The wave field penetrates beyond the resonance layer, and the wave energy is absorbed in both sides of the resonance layer. Experimentally, a finite power is observed on the waveguide array, and the measured transmission coefficient is roughly consistent with calculation. Therefore, low field side interaction also occurs for the typical experimental condition. For electron density roughly higher than 10^{11} cm^{-3}, the injected wave is almost absorbed before the resonance layer.

4.3 Dynamic motion of electrons

Here, a demonstrative shot is presented to confirm the above picture of electron heating. The central cell plasma collapsed during the plug ECRH pulse, and the electron densities at the east and west side plugs varied as shown in Fig. 11 (a). The end plate potentials at both ends also substantially varied (Fig. 11 (b)). The V–I characteristics of the end loss electrons measured simultaneously at both ends are plotted in Fig. 12 for two time intervals (i) and (ii) indicated in Fig. 11 (b). We refer to V–I characteristics as East (i) or West (ii). The values of Φ_{EP} at both ends were nearly equal in the interval (i), and East (i) and West (i) have almost the same features. The situation drastically changed in the interval (ii). East Φ_{EP} became very deep, and west Φ_{EP} was nearly zero. East (ii) is nearly the noise level. This is because little electron heating occurred due to nearly zero electron density at the east plug. The T_L component

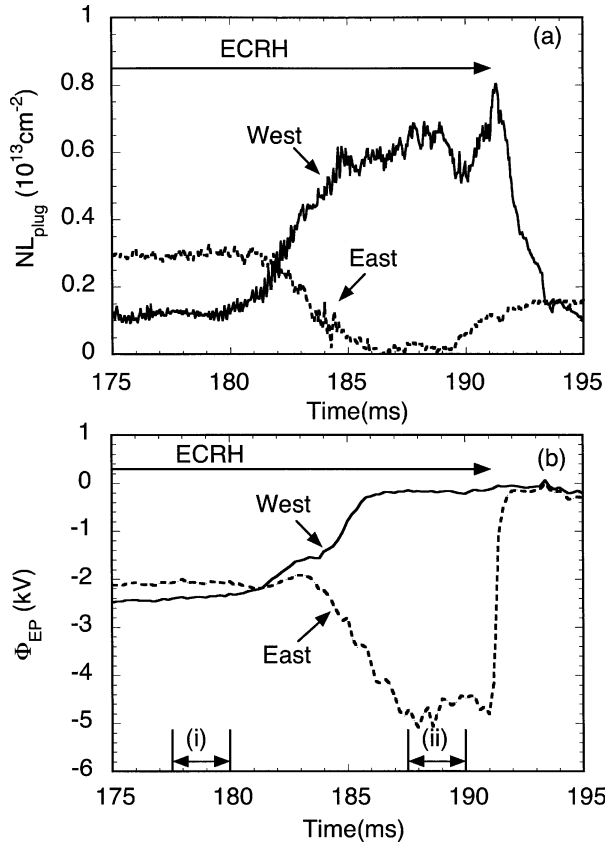

Fig. 11 (a) Line densities at the east and west side plugs are shown. (b) The end plate potentials at the east and west ends are plotted.

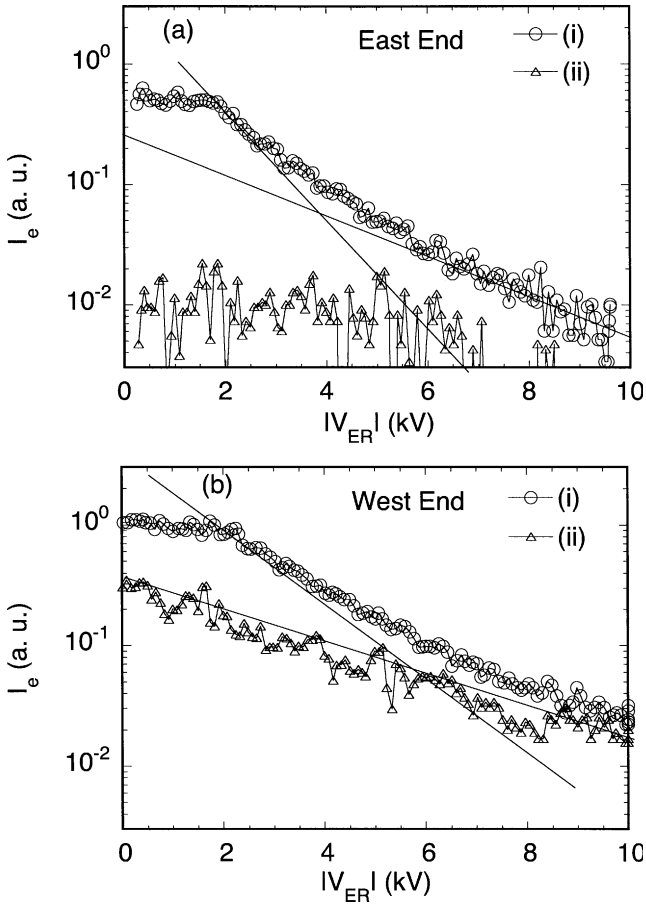

Fig. 12 The V – I characteristics of the end loss electrons measured at both ends simultaneously are plotted for time intervals (i) and (ii) as indicated in Fig. 11.

disappeared from West (ii) while the T_H component was almost the same as that of West (i).

From these observations, it is considered that the origin of the T_L component is electrons trapped between both end plates and that diffusion (2) drives these electrons to the loss region. In the interval (ii), the west Φ_{EP} was nearly zero and electrons could not be trapped between the end plates of both sides. Then, the T_L component originating from these electrons disappeared from West (ii). On the other hand, the T_H component is considered to come from the region III in Fig. 9, and it does not depend on the condition of the opposite side heating. West (ii) supports this. The west electron density exceeded 10^{11} cm^{-3} in the interval (ii), and low field side interaction did not occur. Thus, there was no electron drive to the east side, which resulted in East (ii) of very low signal level. However, because the high field side interaction remained unchanged, the T_H component of West (ii) was generated constantly by diffusion (3).

5. Summary

The high power ECRH experiments at the plug region of GAMMA 10 have been carried out with two steps: high power operation of the existing gyrotrons and installation of a new gyrotron. The attainable plug potential increased almost linearly with the heating power, and a new record of the ion confining potential was achieved in each step. The highest ion confining potential of 2.1 kV for the hot ion mode has been obtained with the new gyrotron. High power heating effect was observed in the characteristics of the end loss electrons, and the scaling between the potential difference from the plug to the end plate and the effective temperature of the end loss electrons was expanded. Absorption of the heating wave in the low field side was shown by using a newly developed code. Measurement of the end loss electrons presented a picture of ECRH-induced velocity space diffusion and resultant dynamic motion of electrons.

References

[1] T. Kariya *et al.*, Phys. Fluids **31**, 1815 (1988).
[2] T. Cho *et al.*, J. Plasma Fusion Res. **80**, 81 (2004).
[3] T. Cho *et al.*, 20th IAEA Fusion Energy Conference, EX/9-6Rd.
[4] T. Cho *et al.*, Nucl. Fusion **43**, 293 (2003).
[5] T. Saito *et al.*, J. Plasma Fusion Res. SERIES **4**, 61 (2001).
[6] T. Saito *et al.*, J. Plasma Fusion Res. **78**, 591 (2002).
[7] T. Saito *et al.*, Trans. Fusion Science and Technology **43**, 167 (2003).
[8] T. Saito *et al.*, Phys. Fluids **B5**, 866 (1993).
[9] T. Saito *et al.*, J. Plasma Fusion Res. **80**, 425 (2004).
[10] T. Saito *et al.*, Fusion Eng. Des. **53**, 267 (2001).
[11] K. Ishii *et al.*, Rev. Sci. Instrum. **60**, 3270 (1989).
[12] M. Yoshida *et al.*, Rev. Sci. Instrum. **74**, 1909 (2003).
[13] T. Saito *et al.*, Trans. Fusion Technol. **35**, 233 (1999).
[14] T. Tamano, Phys. Plasmas **2**, 2321 (1995).
[15] K. Yatsu *et al.*, Nucl. Fusion **39**, 1707 (1999).
[16] M. Inutake *et al.*, Phys. Rev. Lett. **55**, 939 (1985).
[17] T. Cho *et al.*, Phys. Rev. Lett. **86**, 4310 (2001).
[18] T. Rognlien *et al.*, Phys. Fluids **26**, 1545 (1983).
[19] Y. Kiwamoto *et al.*, J. Phys. Soc. Jpn. **58**, 2619 (1989).
[20] T. Kaneko *et al.*, Phys. Rev. Lett. **80**, 2602 (1998).
[21] I. Katanuma *et al.*, Phys. Plasmas **9**, 3449 (2002).
[22] H. Hojo *et al.* J. Plasma Fusion Res. **80**, 175 (2004).
[23] Y. Tatematsu *et al.*, J. Plasma Fusion Res. **80**, 360 (2004).